Available online at www.sciencedirect.com

ScienceDirect

St. Petersburg Polytechnical University Journal: Physics and Mathematics 3 (2017) 1–6

www.elsevier.com/locate/spjpm

Numerical study of spatial-temporal evolution of the secondary flow in the models of a common carotid artery

Yakov A. Gataulin*, Dmitri K. Zaitsev, Evgueni M. Smirnov, Andrey D. Yukhnev

Peter the Great St. Petersburg Polytechnic University, 29 Politekhnicheskaya St., St. Petersburg 195251, Russian Federation

Available online 7 March 2017

Abstract

A numerical study of the secondary flow in two geometrically different models of a common carotid artery has been carried out. One of the models (Model 1) is characterized by a statistically averaged curvature, and the second one (Model 2) is attributed to the maximal curvature of the artery. It was shown that the most intensive swirl occurred at the phase of flow rate decreasing, the maximum values of the swirl parameters were observed at the interface of the cervical and thoracic segments of the artery. This interface is the place where the Dean vortices are transformed into a single vortex forming a swirling flow. The swirl intensity averaged over the systole and characterized by the ratio of the maximal values of the axial and circumferential velocities was evaluated as 0.20 for Model 1 and 0.25 for Model 2. Generally, it was in accordance with the data of clinical measurements.

Keywords: Common carotid artery; Swirling flow; Computational fluid dynamics; Navier–Stokes equations.

Introduction

Carotid arteries are the major blood vessels delivering blood from the heart to the brain. The left common carotid artery originates from the aortic arch and the right one from the brachycephalic artery. Both split into the internal carotid artery, which supplies blood to the brain, and the external carotid artery, which feeds blood to the rest of the head.

Recent studies on the effect of spatial curvature of the common carotid artery on blood flow [1–3] suggest that flows with axisymmetric velocity distributions in the arterial cross-sections virtually never occur. As proved by the results of the computations performed for spatially curved geometry of the common carotid artery in Ref. [1], a flow with a skewed axial velocity profile evolves in the artery, even at a moderate curvature of its cervical segment. The maximum velocity is shifted towards one of the walls due to the development of secondary (cross) flows. The computations performed in [2] for a tortuous carotid model also point to the formation of a flow with a strongly skewed axial velocity profile. Ref. [3] studied the secondary flow in the common carotid artery using an ultrasonic Doppler technique; the authors detected the presence of Dean vortices and a skewed axial velocity profile.

* Corresponding author.
E-mail addresses: yakov_gataulin@mail.ru (Y.A. Gataulin), zaitsev-aero@yandex.ru (D.K. Zaitsev), smirnov_em@spbstu.ru (E.M. Smirnov), a.yukhnev@mail.ru (A.D. Yukhnev).

http://dx.doi.org/10.1016/j.spjpm.2017.02.001

(Peer review under responsibility of St. Petersburg Polytechnic University).

Table 1
Geometrical parameters of the right common carotid artery and the models examined.

Parameter	Notation	Value		
		MRI data	Statistically average model (M1)	Model with maximal physiological tortuosity (M2)
Radius of curvature, mm				
Cervical segment	R_t	40 ± 20	40	20
Thoracic segment	R_c	150 ± 100	150	50
Chord length, mm				
Cervical segment	RT	40 ± 15	40	40
Thoracic segment	RC	60 ± 15	60	60
Angle between the chords, deg	α	25 ± 25	25	25
Angle between the planes in which the cervical and the thoracic segments lie	θ	90 ± 90	90	90

Note: The MRI data was obtained by averaging over 28 healthy volunteers in Ref. [1].

In the present paper, we used the methods of computational fluid dynamics to study the flow in two geometrically different models of the common carotid artery, the statistically average one and the one with maximum physiological tortuosity. We have examined the temporal and spatial evolution of swirling blood flow depending on the curvature parameters of the artery and have drawn conclusions about the structure and features of the blood flow in the tortuosities.

Geometrical model of the common carotid artery

The geometry of the examined models has been constructed from the data obtained by 3D magnetic resonance angiography of blood vessels in the region from the aortic arch to the bifurcation of the carotid artery; the data was averaged over 28 healthy volunteers [1]. According to the technique proposed in [1], the common carotid artery was conventionally divided into the thoracic and the cervical segments; the best-fit circular arcs were used for estimating the centerline radius of curvature (RC) for each of the segments. The estimation was carried out by the least square method.

The geometrical parameters of the considered artery models, as well as the range of physiological data from Ref. [1] are listed in Table 1. The simulation was performed with an inner vessel radius $R = 2.5$ mm.

The choice of the second geometry (Model 2) was governed by the extreme values of the radii of curvature of the cervical and thoracic segments from the physiological range.

The geometry of the common carotid model was constructed in several stages using the DesignModeler software that is a part of the ANSYS Workbench platform. First, arcs with a common intersection point at the origin were constructed in mutually perpendicular planes XY and XZ: the first arc corresponded to the cervical segment of the common carotid artery and the second one to the thoracic one (Fig. 1). Each arc was described by the radius of curvature and the chord length. Equally spaced points were then plotted on the arcs, and a smooth space curve was drawn through the points using the 3D-Spline tool. This curve served as an axis for the common carotid model. As the final stage, a cylindrical surface simulating the inner wall of the artery was constructed.

Mathematical model

Three-dimensional unsteady Navier–Stokes equations were solved in order to simulate the flow in the common carotid artery. The computations were performed with the ANSYS CFX code by the control volume method with second-order accuracy in space and time.

A uniform velocity profile and a variation in the mean flow velocity during the cycle (which will be demonstrated below by the dotted curve in Fig. 5) were specified at the inlet boundary. The mean velocity curve was obtained from the flow rate curve reproducing the results of clinical measurements of blood flow in healthy volunteers by phase-contrast magnetic resonance imaging (MRI) [4]. The cycle period $T = 1$ s. The velocity increase phase makes up 15% of the total cycle time. The maximum mean flow velocity for the period $V_{b\max} = 0.7$ m/s. The phase of mean flow velocity decrease is characterized by the presence of three local velocity maxima associated with the motion of the pulse wave through the vessels. A constant pressure was specified at the outlet

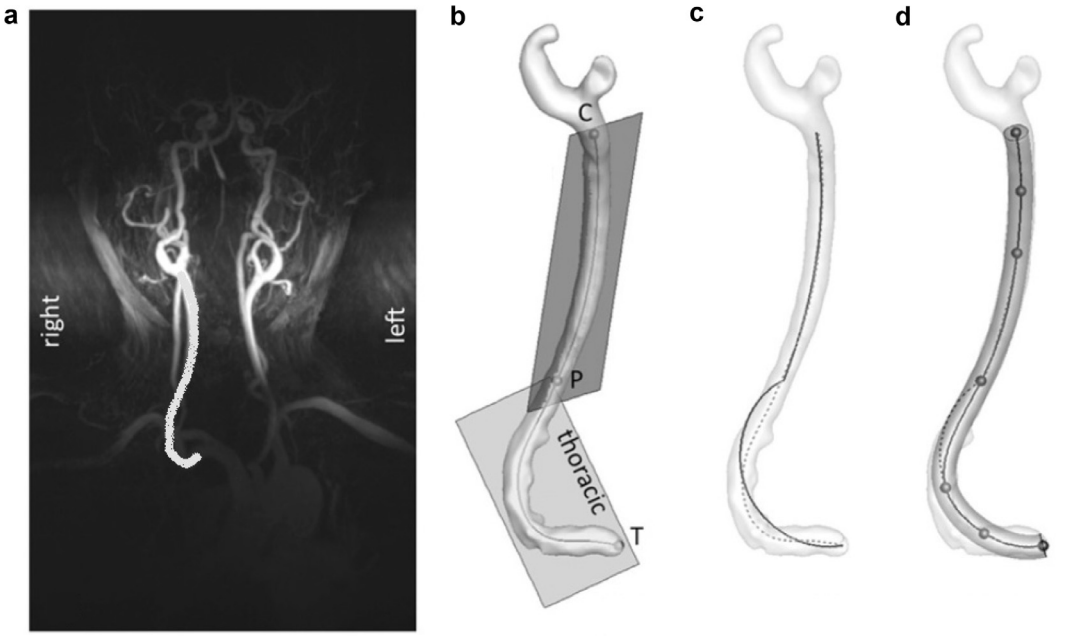

Fig. 1. Stages of constructing a geometrical model of the right common carotid artery: *a* is the MR image of the blood vessel network (the left and the right common carotid arteries are marked); *b* is the right common artery divided into segments (*T* is the thoracic and *C* is the cervical segment); *c* is the vessel axis (dashed line), thoracic and cervical segments (solid line); *d* is the common carotid model obtained by smoothing the thoracic and cervical arcs with subsequent construction of the cylindrical surface [1].

boundary of the vessel model. The no-slip condition was imposed on the walls.

The computations were performed for a liquid whose properties were similar to blood: the dynamic viscosity coefficient $\mu = 0.004$ Pa s, the density $\rho = 1000\,\text{kg/m}^3$. The maximum Reynolds number per cycle for these parameters is

$$\text{Re} = 2\rho V_{b\ \max} R/\mu \approx 900$$

and the Womersley number is

$$W_O = R\sqrt{2\pi\rho/\mu T} \approx 3.$$

Choice of the computational mesh

The computational mesh for the common carotid model was constructed in the ANSYS Meshing (an application of the ANSYS Workbench environment) using the Body Sizing and Inflation tools. The first of these tools sets the type of the mesh elements and their maximum size, and the second sets the clustering of the mesh to the model's wall. The computational mesh consisted of prismatic elements whose maximum size was selected based on a mesh convergence test.

Fig. 2 shows two of the four computational meshes in the cross-section of the artery model. We used the coarsest (with a total number of 43,000 elements) and the most refined (with 450,000 elements) meshes for the mesh convergence test.

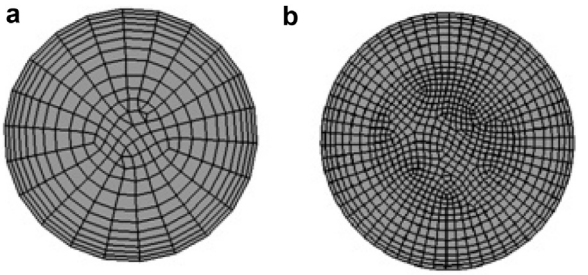

Fig. 2. Images of the coarsest (*a*) and the finest (*b*) computational meshes in the cross-section of the artery model.

Fig. 3 shows the axial velocity field in the cross-section positioned in the middle of the cervical segment. The field was computed using the two meshes in the steady-state problem case for artery model 2 with the mean flow velocity $V_b = 0.7$ m/s (this value corresponds to the maximum velocity per cycle in case of unsteady problem setting).

The results of the mesh convergence test allowed to reach a general conclusion that the velocity field for the coarsest mesh was significantly different from the fields obtained for the other three meshes (86,000, 172,000, and 450,000 elements). However, the results

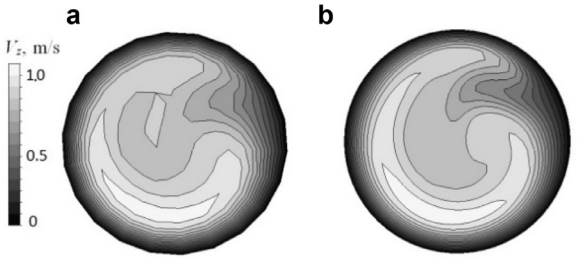

Fig. 3. Axial velocity fields in the middle of the cervical segment (cross-section), computed for the coarsest (*a*) and the finest (*b*) meshes.

for the second and the third grids were very similar: the difference did not exceed 5%. As a result, the grid with 450,000 total elements was chosen for unsteady computations.

A test was also performed on the time-step sensitivity of the obtained results. The solutions compared were obtained with the steps of 0.005, 0.010 and 0.020 s. As a result, it was found that the solution varied only slightly with decreasing time steps in the specified range; because of this, the main computations were carried out only with a step of 0.01 s.

Computational results

The computations revealed that Dean vortex pairs in which the fluid rotated in opposite directions formed in the thoracic segment of the common carotid artery. The Dean vortices in Fig. 4 are visualized by Q-criterion isosurfaces; they have the form of two structures of similar shape, elongated along the outer wall of the vessel model. Upon entering the cervical segment of the common carotid, the Dean vortices were transformed into a single vortex generating a swirling flow. The most intense swirling was generated in the junction between the thoracic and cervical segments. The swirl attenuated downstream, and a second vortex emerged approximately in the middle of the cervical segment, gradually increasing in size along the length of the vessel.

Two parameters were used to characterize the intensity of the swirling flow: the integral swirl parameter *S*,

$$S = \frac{\int V_\varphi V_z r^2 dr}{R \int V_z^2 r dr},$$

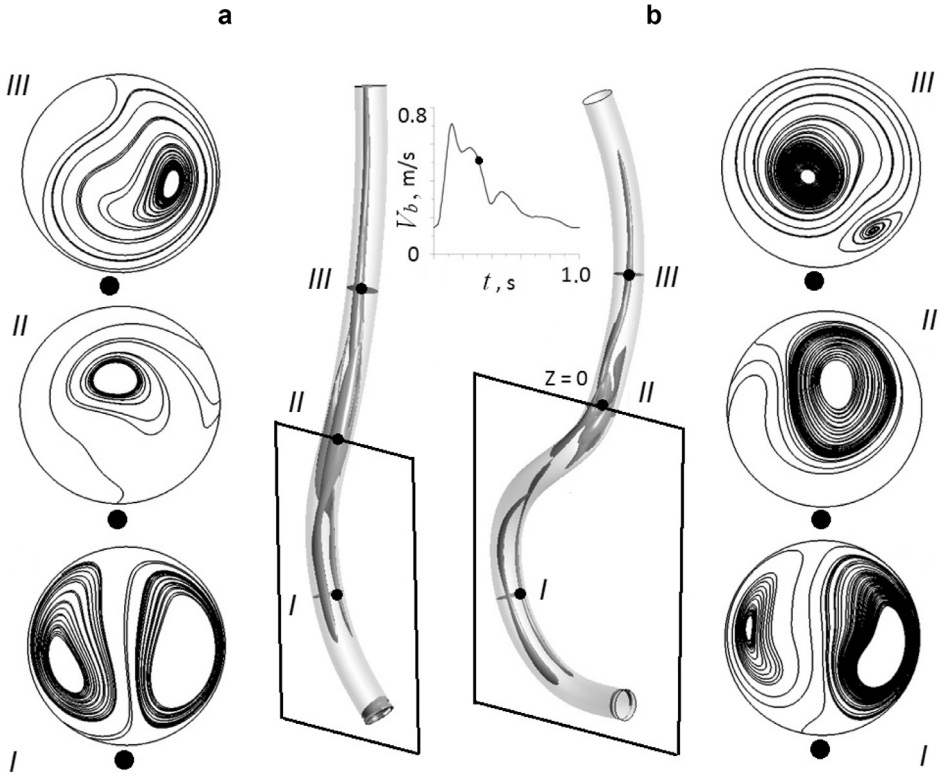

Fig. 4. Q-criterion isosurfaces in the phase of flow rate decrease ($t = 0.3$ s) and the flow lines in the three cross-sections (*I*, *II*, *III*) for Model 1 (*a*) and Model 2 (*b*); the inset shows the dynamics of the mean flow velocity per cycle, the time $t = 0.3$ s is marked with a dot.

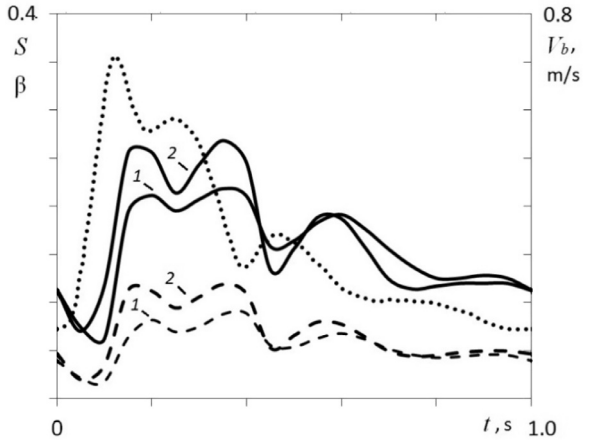

Fig. 5. Variation of the two swirl parameters during the cycle: S (dashed lines) and β (solid lines) in the cross-section in the middle of the cervical segment for models 1 and 2, in comparison with the dynamics of the mean flow velocity (dotted line).

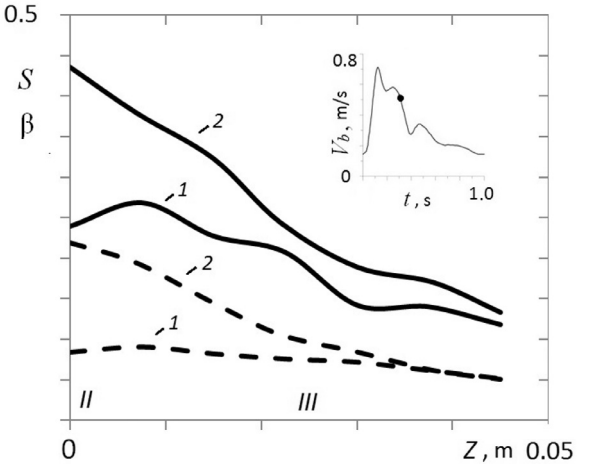

Fig. 6. Variation of the swirl parameters over the length of the cervical segment: S (dashed lines) and β (solid line) at time $t = 0.3$ s for models 1 and 2 of the common carotid artery; the inset is identical to the one shown in Fig. 4.

which is defined as the dimensionless angular momentum flux, and the swirl parameter β widely used in practice:

$$\beta = \frac{V_{\varphi\,\max}}{V_{z\,\max}},$$

which is defined as the ratio between the maximum peripheral velocity to the maximum axial velocity. In these formulae r is the radial coordinate; R is the vessel radius; V_φ and V_z are the circumferential and the axial velocities.

Fig. 5 shows the variation of the two swirl parameters during the cycle for both of the examined models. It can be seen that the most intense swirl occured during systole (from about 0.17 s to 0.40 s). During this time interval $S \approx 0.08$ and $\beta \approx 0.2$ for the statistically average model, while the swirl intensity was higher by about 30–50% for the model with maximum physiological tortuosity. Notably, the β/S ratio was approximately constant for both models for most of the cycle and amounted to 2.0–2.5.

Fig. 6 shows the variation of the swirl parameters along the length of the cervical segment of the artery model. It is characterized by a smooth decrease that is almost linear in some regions. Despite a pronounced difference between the swirl intensities obtained for the two models in the beginning of the cervical segment ($S \approx 0.1$, $\beta \approx 0.2$ for Model 1; $S \approx 0.2$, $\beta \approx 0.45$ for Model 2), the intensities of the swirling flow leveled by the end of the cervical segment and were characterized by the values $S \approx 0.05$, $\beta \approx 0.1$. These values are recommended for use as inlet conditions in setting a numerical problem on computing the blood flow in the carotid bifurcation.

Conclusion

Swirling flow in the tortuous carotid artery is formed under the influence of the spatial curvature of the artery and the pulsating nature of the flow. The most intense swirl is formed during the flow rate decrease phase at the junction of the thoracic and cervical segments, where the Dean vortices, typical for flow in curvilinear tubes, are transformed into a single vortex generating the swirling flow. As the swirl attenuates, a second vortex re-emerges downstream. The mean swirling intensity per systole (determined by the ratio of the maximum circumferential velocity to the maximum axial velocity) amounts to 0.20 for the model of the statistically average common carotid artery and to 0.25 for the model with maximum physiological tortuosity, which agrees with the clinical results [5].

Acknowledgment

The study was carried out with the financial support of the Russian Foundation for Basic Research (Grant no. 15-01-07923).

References

[1] A. Manbachi, Y. Hoi, B.A. Wasserman, E.G. Lakatta, D.A. Steinman, On the shape of the common carotid artery with implications for blood velocity profiles, Physiol. Meas. 32 (12) (2011) 1885–1897.

[2] Ya.A. Gataulin, A.D. Yukhnev, M.A. Popov, D.I. Kurapeyev, Numerical simulation of the blood flow in the common carotid artery with *S*-shaped tortuosity, Biotekhnosfera. 5 (1) (2013) 27–33.

[3] M.D. Ford, Y.J. Xie, B.A. Wasserman, D.A. Steinman, Is flow in the common carotid artery fully developed? Physiol. Meas. 29 (11) (2008) 1335–1349.

[4] Y. Hoi, B.A. Wasserman, Y.J. Xie, Characterization of volumetric flow rate waveforms at the carotid bifurcations of older adults, Physiol. Meas. 31 (3) (2010) 291–302.

[5] V.P. Kulikov, R.I. Kirsanov, S.V. Zasorin, Dopplerografic recording the phenomenon of the screw blood motion in the human common carotid arteries, Ultrazvukovaya funktsionalnaya diagn. 2 (1) (2006) 96–100.